# Pitfalls of choosing an order parameter for rare event calculations

Bradley M. Dickson,[a] Dmitrii E. Makarov, and Graeme Henkelman[b]
*Department of Chemistry and Biochemistry and Institute for Computational Engineering and Sciences,*
*University of Texas at Austin, Austin, Texas 78712, USA*

The mechanism of rare events in complex systems can be found by sampling dynamical paths that connect stable states. To calculate a rate using transition paths, an order parameter is required to describe the progress of the reaction and to distinguish the initial and final states. In this work, we compare two implementations of transition path sampling for Langevin paths, one for which paths are sampled in configuration space and the other in the space of the random variables that describe the thermostat. These two approaches are found to give different rates for the rearrangement of a seven-particle cluster despite the fact that both are formally exact. The difference is understood in terms of how efficiently the methods sample states along the order parameter. The more efficient approach takes the system to unexpected states that are allowed by a poor choice of order parameter. While transition path sampling is formally correct, we show how mistakes can be made when the system escapes to unknown states along an order parameter represented in terms of collective variables. © *2009 American Institute of Physics.* [DOI: 10.1063/1.3204008]

## I. INTRODUCTION

In chemical and material systems a rare event can be characterized by a transition from one stable state to another. Between events, the system waits for an opportunistic fluctuation to cause a transition. Within a state, the dynamics of the system are dominated by atomic vibrations on the femtosecond time scale. Transitions from state to state, on the other hand, can take place on much longer times, from microseconds to seconds. It is this disparity of time scales that constitutes the rare event problem: following the dynamics of chemical systems requires femtosecond accuracy while interesting transitions often require seconds of accumulated time.

Several approaches have been used to overcome the rare event problem. The transition state theory (TST) approximation effectively replaces the problem of dynamics by that of statistical mechanics. Specifically, the TST rate is proportional to the equilibrium probability for the system to reach a bottleneck region or transition state. In recent years, a variety of path sampling techniques have been proposed which do not, in principle, require *a priori* knowledge of the transition states that control the rate of rare events.[1–5] Moreover, path sampling makes no approximations and, again in principle, yields the exact transition rate. Path sampling, like some applications of TST or Kramers theory,[6–8] requires the specification of an order parameter (OP) or progress coordinate. An advantage of path sampling over TST is that the OP need not characterize a physical reaction coordinate, it must only separate reactants and products.

In this paper, we investigate the efficiency and accuracy of path sampling methods for the calculation of reaction rates. We consider rearrangements of a seven-particle

Lennard-Jones (LJ) cluster confined to a surface, a model system that has been used in previous calculations to test path sampling methods.[1,9] We use the same OP in these previous calculations to compute the rates of such rearrangements with two path sampling schemes, transition path sampling (TPS) (Ref. 1) and noise sampling (NS).[10,11] We find that the TPS rate constant does not agree with that from NS or a harmonic TST calculation. The discrepancy is traced to a poor choice of OP; while it successfully separates the initial and final states of the reaction it fails to uniquely identify the initial state. Even with such a simple model system, this pitfall was not obvious in our calculations or to others using the same OP.[1] Such problems are expected to be even harder to detect in larger systems such as those involving complex reactions in biological molecules.

## II. BACKGROUND

### A. Transition state theory

TST is one of the earliest formalisms for describing rare events in chemistry.[12,13] The TST rate constant is given by

$$k_{TST} = \frac{\left\langle \frac{1}{2} |\dot{\lambda}| \delta(\lambda^{\dagger} - \lambda(x)) \right\rangle}{\langle h_A(x) \rangle}, \tag{1}$$

where $\langle \cdot \rangle$ is an expectation in the canonical ensemble and $h_A$ is the indicator function for the initial stable state $A$. $h_A$ is defined in terms of a collective coordinate or OP $\lambda(x)$. When this OP is chosen to separate reactants from products, the indicator function is $h_A(x) = \Theta(\lambda^{\dagger} - \lambda(x))$, where $\Theta(\lambda)$ is the Heaviside step function, $\lambda^{\dagger}$ is the boundary of $A$, and $|\dot{\lambda}|$ is the rate at which the OP as trajectories cross the boundary of $A$, 1/2 of which cross in the forward direction.

The TST rate overestimates the true rate and is variational with respect to the choice of the boundary or dividing surface. The surface of maximum free energy will give a

---
a)Electronic mail: bradley.dickson@ens-lyon.fr.
b)Electronic mail: henkelman@mail.utexas.edu.

TST rate that is as close to the true rate as possible.[14] Ideally $\lambda(x)=\lambda^{\dagger}$ defines the optimal dividing surface, yielding the lowest TST rate constant. This is rarely possible and choosing a suitable OP or reaction coordinate is the challenge for applying of TST and Kramers theory.

In many cases, the harmonic approximation to TST (hTST) gives a good estimate of $k_{\text{TST}}$. hTST is valid when the potential energy can be adequately approximated as a harmonic oscillator in the thermally accessible region around the minimum and in the plane which passes through the saddle point normal to the negative curvature mode. Using hTST the rare-event problem is reduced to searching for saddle points[15,16] and the need to specify an OP is removed. The harmonic rate constant is

$$k_{\text{hTST}} = \frac{\Pi_{i=1}^{N} \nu_i}{\Pi_{j=1}^{N-1} \nu_j} e^{-\beta \Delta E}, \tag{2}$$

where there are $N-1$ real vibrational frequencies at the saddle and $N$ at the minimum. $\Delta E$ is the energy difference between the saddle configuration and the minimum, $\nu_i$ and $\nu_j$ are the normal mode frequencies at those stationary points, respectively, and $\beta=1/(k_B T)$, where $k_B$ is Boltzmann's constant and $T$ is the temperature.

## B. Path sampling

While hTST is often adequate for solids and gas-phase reactions, many molecular systems including those involving biological molecules feature rugged energy landscapes with multiple local minima and saddle points along reaction pathways so that they cannot be described within a harmonic approximation. Path sampling was developed for such situations. This method requires an OP $\lambda(x)$ which separates reactants from products but does not necessarily define a good transition state.

TPS computes the flux-position correlation function of the form[17]

$$k(t) = \frac{\langle \dot{\lambda}(x(0)) \delta(\lambda^{\dagger} - \lambda(x(0))) h_B(x(t)) \rangle}{\langle h_A(x(0)) \rangle}, \tag{3}$$

where the product state indicator function $h_B(x)=1-h_A(x)$ and the averaging is performed over trajectories $x(t)$. The exact rate $k$ is the plateau value of $k(t)$ at times longer than the vibrational time but shorter than that of the rare event itself, $1/k$.

In order to cast Eq. (3) on an ensemble of paths we note that with

$$\dot{h}_A(x(0)) = -\delta(\lambda^{\dagger} - \lambda(x(0))) \dot{\lambda}(x(0)) \tag{4}$$

and

$$-\langle \dot{h}_A(x(0)) h_B(x(t)) \rangle = \langle h_A(x(0)) \dot{h}_B(x(t)) \rangle, \tag{5}$$

Eq. (3) becomes

$$k(t) = \frac{\langle h_A(x(0)) \dot{h}_B(x(t)) \rangle}{\langle h_A(x(0)) \rangle}. \tag{6}$$

Factoring Eq. (6) in terms of paths of a fixed length $\tau$ produces
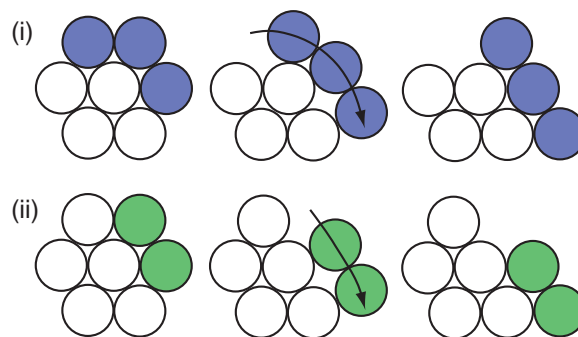


FIG. 1. The initial, saddle, and final configurations for the (i) three particle and (ii) two particle slides.

$$k(t) = \frac{\langle h_A(x(0)) \dot{h}_B(x(t)) \rangle}{\langle h_A(x(0)) h_B(x(\tau)) \rangle} \frac{\langle h_A(x(0)) h_B(x(\tau)) \rangle}{\langle h_A(x(0)) \rangle}, \tag{7}$$

where $0 \le t \le \tau$. Now the calculation can be separated into the two factors in Eq. (7), (i) the flux among trajectories that start in stable state $A$ and transition to stable state $B$ in time $\tau$ and (ii) the probability of observing such a trajectory. These two terms are called the "flux" and "probability" factors, respectively.[1] When paths can be sampled ergodically, the rate constant is independent of the choice of $\lambda$ so long as it uniquely identifies the reactants and products.

## III. RESULTS AND DISCUSSION

### A. The model

To compare methods of calculating rates we have investigated the rearrangements of a seven-particle cluster confined to a surface interacting via a LJ potential

$$V = \sum_{i<j} 4\epsilon \left[ \left( \frac{\sigma}{r_{ij}} \right)^{12} - \left( \frac{\sigma}{r_{ij}} \right)^{6} \right], \tag{8}$$

where $r_{ij}$ is the distance between particles $i$ and $j$. Reduced units are used throughout: time in units of $\tau_0=\sqrt{m\sigma^2/\epsilon}$, energy in units of $\epsilon$, and distance in units of $\sigma$. We describe the cluster dynamics through Langevin's equation of motion

$$m\ddot{x}(t) = -m\gamma\dot{x}(t) - \nabla V(x(t)) + f(t), \tag{9}$$

where $\gamma$ is the friction and $m$ is the mass. The stochastic force $f(t)$ is a delta-correlated normally distributed random variable with $\langle f(t) \rangle = 0$ and

$$\langle f(t) f(t') \rangle = 2k_B T \gamma \delta(t - t') m. \tag{10}$$

Molecular dynamics were calculated using the Langevin integrator of Ref. 18 where the thermal energy $k_B T=0.05\epsilon$, the friction $\gamma=1/\tau_0$, and the time step $dt=0.02\tau_0$.

The two processes with the lowest energy barriers from the ground state of the cluster were chosen for our comparison, corresponding to two and three particle slides shown in Fig. 1.

### B. Harmonic TST rates

The rates of these processes were calculated using hTST. First we found the saddle point for each with the climbing image nudged elastic band method.[16] The hTST rate constant

TABLE I. hTST prefactor, barrier $\Delta E$, and rate $k_{hTST}$ for the (i) three particle and (ii) two particle slides.

| Process | Prefactor | $\Delta E$ | $k_{hTST}$ |
|---|---|---|---|
| i | 2.98 | 1.4975 | $2.93 \times 10^{-13}$ |
| ii | 2.77 | 1.4946 | $2.89 \times 10^{-13}$ |

of Eq. (2) was calculated from the barrier height and the normal mode frequencies at the initial minimum and at the saddle point. The normal modes were determined by finite difference. The harmonic prefactors and the activation energies for the two and three particle slides are listed in Table I along with the rate constants. Our activation energies are the same as those tabulated in Ref. 9.

## C. Transition path sampling rate

Dellago *et al.* calculated the rates of rearrangement for the seven-particle cluster from TPS. We followed their procedure, which is outlined in Ref. 1, as closely as possible. In particular, we used the functional form of their OP to characterize reactants, products, and the extent of reaction. This OP is the mean squared distance between a configuration $x$ and the minimized product state geometry $x_p$,

$$\lambda_p = \frac{1}{7} \sum_{i=1}^{7} (U x_i - x_{p_i})^2, \qquad (11)$$

where the rotation $U$ is chosen to minimize $\lambda_p$ for a given $x$. The initial state $A$ and final state $B$ are defined as the set of $x$ satisfying $\lambda_p > 0.8$ and $\lambda_p < 0.1$, respectively. These values were chosen to be outside of the fluctuations of long thermal trajectories from each state. Indicator functions for the initial and final states are $h_A(x) = 1 - \theta[0.8 - \lambda_p(x)]$ and $h_B(x) = \theta[0.1 - \lambda_p(x)]$.

A Monte Carlo algorithm was used to sample reactive paths. Two types of moves were used with equal probability, shooting and reptation moves. A shooting move proceeds by first randomly selecting a point along a reactive path $x(t)$ and launching a new segment in either the forward or backward time direction. The new integrated path segment replaces the old segment if the whole path remains reactive. For a reverse shooting move, the momenta of the randomly selected phase point are reversed and a new trajectory segment is integrated. The momenta along this new segment are reversed and the old segment is replaced if this new one reaches the initial state. Forward shooting moves were attempted as often as backward ones.

Reptation moves translate the path forward or backward in time. A time $t^*$ is chosen uniformly on the interval $[0, \tau]$, and for a forward reptation, a $t^*$-length segment is appended to the end of the path. At the same time, $t^*$ time is removed from the beginning of the path so the total length is conserved. The path is accepted if $h_A(x(0))h_B(x(\tau)) = 1$. The reverse time reptation move follows this same procedure but adds a new trajectory segment of length $t^*$ to the beginning of the path and removes a segment at the end.

Calculations for the factors in Eq. (7) were carried out with paths consisting of 199 steps for the three particle
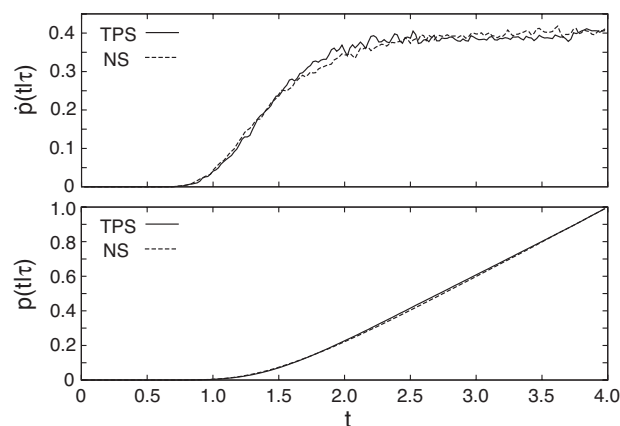


FIG. 2. The frequency factors for TPS and NS give the reactive flux within the $\tau$-length path ensemble. The two methods have the same plateau at 0.4.

slide—the process with the highest hTST rate. The reference state $x_p$ in the OP $\lambda_p$ is the final state of process (i) in Fig. 1. We determined the frequency factor by sampling reactive trajectories and collecting the number of such paths in state $B$ at time $t$ to construct the conditional probability

$$p(t|\tau) = \frac{\langle h_A(x(0)) h_B(x(t)) \rangle}{\langle h_A(x(0)) h_B(x(\tau)) \rangle}. \qquad (12)$$

The numerical time derivative of this distribution is the frequency factor

$$\dot{p}(t|\tau) = \frac{\partial p(t|\tau)}{\partial t} = \frac{\langle h_A(x(0)) \dot{h}_B(x(t)) \rangle}{\langle h_A(x(0)) h_B(x(\tau)) \rangle}. \qquad (13)$$

With $\tau$ chosen suitably long, this frequency factor plateaus after an initial relaxation time here at 0.4, as seen in Fig. 2.

The probability factor is evaluated from the distribution $p(\lambda_p)$

$$= \frac{\iint h_A(x(0)) \delta(\lambda_p - \lambda_p(x(\tau))) P[x(t)] e^{-\beta H(\Gamma_0)} D[x(t)] d\Gamma_0}{\iint h_A(x(0)) P[x(t)] e^{-\beta H(\Gamma_0)} D[x(t)] d\Gamma_0}, \qquad (14)$$

where $H(\Gamma_0)$ is the Hamiltonian at the initial phase point $\Gamma_0$ and

$$P[x(t)] = e^{-1/4 \gamma k_B T \int_0^\tau [m \ddot{x}(s) + m \gamma \dot{x}(s) + V(x(s))]^2 ds} \qquad (15)$$

assigns a weight to each path according to Langevin's equation. Equation (14) is the probability of finding a $\tau$-length path that begins in state $A$ and ends at the value of the OP $\lambda_p$. With this, the probability of finding a $\tau$-length path that ends in the product state is

$$P(\tau) \equiv \frac{\langle h_A(x(0)) h_B(x(\tau)) \rangle}{\langle h_A(x(0)) \rangle} = \frac{\int_{\lambda_p \in B} p(\lambda_p) d\lambda_p}{\int_{\lambda_p} p(\lambda_p) d\lambda_p}. \qquad (16)$$

The distribution $p(\lambda_p)$ is evaluated with umbrella sampling.[19] The phase space is broken into small regions according to $\lambda_p$ and histograms are built on each region. These histograms overlap each other so that they can be matched to produce the distribution along $\lambda_p$. The only difference between this calculation and standard umbrella sampling is that instead of running molecular dynamics confined to each region along

TABLE II. Rate constants and 95% confidence intervals from TPS and NS calculations at equal computational cost. The OP of $\lambda_p$ is the squared distance from the product state. $P(\tau)$ is the average probability factor and $\dot{p}(t|\tau)$ is the frequency factor.

| OP | Method | $\dot{p}(t|\tau)$ | $P(\tau)/10^{-13}$ | $k_{AB}/10^{-13}$ |
|---|---|---|---|---|
| $\lambda_p$ | TPS | 0.39 | 9.2 | $3.60 \pm 0.18$ |
|  | NS | 0.40 | 8.0 | $3.20 \pm 0.19$ |

$\lambda_p$ we sample paths of length $\tau$ that start in state $A$ and end in the specified region of $\lambda_p$. The histogram records the position of the end point of the trajectories in each region.

For this calculation, the OP $\lambda_p$ was divided into 15 bins with one fourth of the total bin width overlapping on the high side and one fourth overlapping on the low side. The range of $\lambda_p$ was $[0,1.6]$. The calculation of the probability factor was repeated 20 times to gather statistics and the total computational cost was $6.5 \times 10^{10}$ force calls. This amounts to $3 \times 10^6$ path moves per simulation. With this approach we find that the rate constant (see Table II) is 25% higher than that of hTST—well outside the 5% statistical uncertainty.

It is somewhat surprising that the TPS rate is higher than the hTST rate since TST overestimates the true rate. The discrepancy could be influenced by the harmonic approximation or some nonlocal effects,[20] but as will be seen below, an alternative implementation of TPS produces a rate that is much closer to the hTST value.

### D. Noise sampled paths

To test the accuracy of our TPS calculation, we recalculate the rate of transition using another approach where paths are sampled in the space of the Langevin stochastic force or noise.[11] In this NS method, we start with an initial, reactive $\tau$-length path that is discretized as[18]

$$x_{i+1} = x_i + c_1 v_i \Delta t + c_2 a_i \Delta t^2 + \delta x_i,$$
$$v_{i+1} = c_0 v_i + (c_1 - c_2)a_i \Delta t + c_2 a_{i+1}\Delta t + \delta v_i, \qquad (17)$$

where $a_i = -\nabla V(x(t_i))/m$ and

$$c_0 = e^{-\gamma \Delta t}; \quad c_1 = \frac{1-c_0}{\gamma \Delta t}; \quad c_2 = \frac{1-c_1}{\gamma \Delta t}. \qquad (18)$$

The time step is given by $\Delta t = \tau/n$, where $n$ is the number of discrete steps along the path. The weight of this path is

$$P[x(t)] = \frac{1}{2\pi \sigma_x \sigma_v \sqrt{1-c_{rv}^2}} \prod_{i=0}^{n} e^{-g(\delta x_i, \delta v_i)/2(1-c_{rv}^2)}, \qquad (19)$$

where

$$g(\delta x_i, \delta v_i) = \left(\frac{\delta x_i}{\sigma_x}\right)^2 + \left(\frac{\delta v_i}{\sigma_v}\right)^2 - 2c_{rv}\frac{\delta x_i}{\sigma_x}\frac{\delta v_i}{\sigma_v} \qquad (20)$$

and

$$\sigma_x^2 = \Delta t \frac{k_B T}{m\gamma}[2 - (3 - 4e^{-\gamma \Delta t} + e^{-2\gamma \Delta t})/\gamma \Delta t],$$

$$\sigma_v^2 = \frac{k_B T}{m}[1 - e^{-2\gamma \Delta t}], \qquad (21)$$

$$c_{rv}\sigma_x\sigma_v = \frac{k_B T}{m\gamma}[1 - e^{-\gamma \Delta t}]^2.$$

The path is sampled with a shooting move by randomly choosing time slices and drawing a new noise value according to Eq. (19). In our simulations, a random number of indices between 1 and 10 are chosen for a change in noise at each iteration. If the initial point is chosen, it is displaced as in a standard Monte Carlo sampling. Equation (17) is then used to integrate the new trial path $y(t)$, which is accepted with the probability

$$P_{\text{acc}} = \min\{1, h_A(y(0))h_B(y(\tau))\}. \qquad (22)$$

This method differs from Ref. 10 in that the equation of motion is not restricted to the high friction limit.

To facilitate the sampling of different escape times between $0 \le t \le \tau$ a reptation move was used. This move allows time steps to be added to the beginning or end of the path without requiring time reversibility by sampling paths that are longer than the length of interest while only viewing a $\tau$-length segment of each long path. The reptation move consists of sliding the window of visibility along the path where the newly visible section of path can be exchanged for the old one according to Eq. (22).

The NS algorithm in Ref. 11 is amended only slightly because of this window and only to improve efficiency. Trajectories are only needed prior to the $t = \tau$ edge of the reptation window. Altering noise beyond the trailing edge of the reptation window does not change the visible part of the path. When the reptation window is moved toward the beginning of the path, the reptation move requires no force evaluations. When the reptation window is moved forward toward the end of the path, integration is carried out only between the old $x(t=\tau)$ location and the new trial location $y(t=\tau)$.

The frequency factor was calculated with the same definitions for states $A$ and $B$ and is shown in Fig. 2. TPS and NS produce the same reactive flux in the reactive path ensemble. Twenty observations of the probability factor were made. Path moves of NS and reptation were made with equal probability. The simulations were capped at a total of $6.5 \times 10^{10}$ force calls to match the TPS calculation. The results of the NS calculation are given in Table II.

### E. Comparison of the rate calculations

The rate constant from NS paths is found to be higher than the hTST rate but considerably closer to it than the TPS rate. What is more worrisome is that the NS and TPS rates are significantly different despite the fact that both are formally exact.

The frequency factors for TPS and NS are the same and not the source of the difference in rate. The difference be-
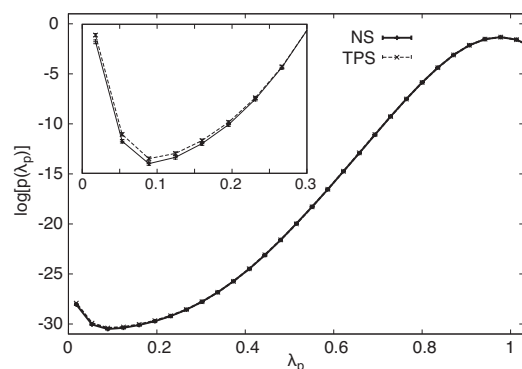
FIG. 3. The probability that a path from the initial state terminates at the given value of $\lambda_p$.

tween the two sampling methods is thus in the probability factor, which quantifies the exponential dependence of the rate constant on the free energy landscape. Figure 3 shows the logarithm of the probability factor [$p(\lambda)$ from Eq. (14)] along the OP $\lambda_p$. The difference between the NS and TPS calculations is very small; it is only noticeable in the enlarged inset of Fig. 3 at small values of $\lambda$. It is this small difference which results in the discrepancy between the TPS and NS rates.

## F. A second order parameter

The difference between the TPS and NS calculations was found by observing reactive trajectories and noticing that some of the initial state configurations were not the compact seven-particle cluster (the initial configuration for the mechanisms in Fig. 1). The initial state for the path sampling simulations is defined by $\lambda_p > 0.8$, which is the set of configurations for which the mean squared distance from the product state is greater than 0.8. This definition turns out to be too general; there is more than one potential energy minimum within this distance of the product state. To resolve the different states, we introduce a second OP $\lambda_r$, which is defined in the same way as $\lambda_p$ except using the compact reactant state as the reference from which the mean-squared distance is calculated,

$$\lambda_r = \frac{1}{7}\sum_{i=1}^{7}(Ux_i - x_{r_i})^2. \tag{23}$$

Figure 4(b) shows the free energy landscape as a function of the two OPs $\lambda_p$ and $\lambda_r$. Our product state was chosen to be the region $\lambda_p < 0.1$. A single free energy minimum is found in this region near $(\lambda_p, \lambda_r) = (0.0, 1.0)$, which corresponds to the final state of the desired three-particle slide [Fig. 1(i)]. Our reactant state was chosen to be in the region $\lambda_p > 0.8$. The desired compact initial state is found in this region near (0.9,0). What is interesting is the second initial state at (0.8,1.0). This local minimum, which is the product of the two-particle slide [Fig. 1(ii)], does not appear in the free energy profile along $\lambda_p$ shown in Fig. 4(a). The one dimensional projection onto the single coordinate $\lambda_p$ hides structure in the other coordinate(s). In fact, there was no way to detect this alternate initial state from the path sampling calculation without looking at the configurations directly.
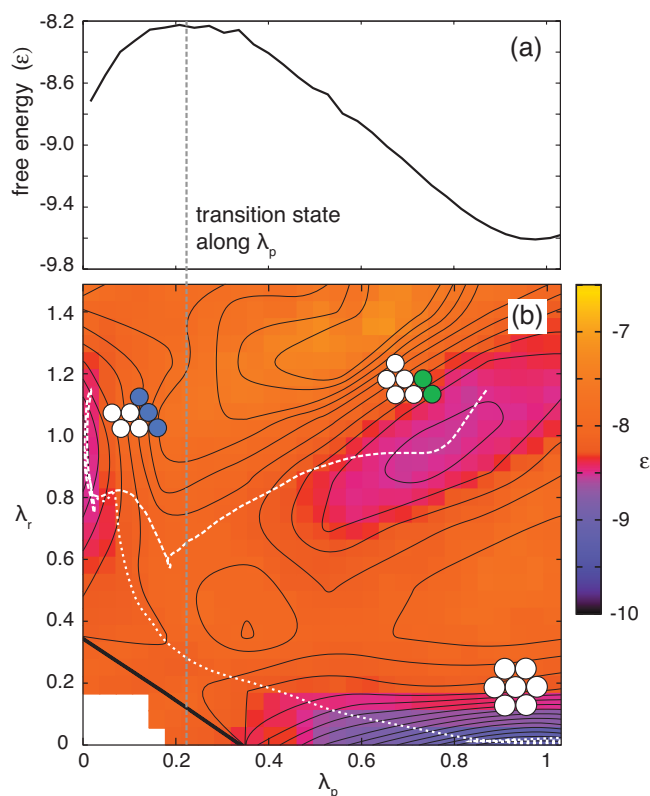


FIG. 4. (a) The free energy calculated along one OP $\lambda_p$ for the rearrangement of the seven-particle cluster. (b) The free energy in two OPs, $\lambda_p$ and $\lambda_r$. Contours are spaced by $2k_BT$. The two paths shown (dashed white lines) are considered reactive using the $\lambda_p$ OP, but only one (the lower path) connects to the intended initial state. Using the second OP $\lambda_r$ distinguishes between the paths.

With a clearer picture of the free energy surface in two OPs we can understand the difference between our TPS and NS rate calculations. In both cases, reactants and products were defined by $\lambda_p > 0.8$ and $\lambda_p < 0.1$, respectively. Now we can see that there are (at least) two reaction mechanisms shown as white dashed trajectories in Fig. 4(b). The combined rate of these processes should be the result of our path sampling calculations when the path space is sampled ergodically. It is then understandable that the path sampling rate is higher than the TST rate of the single three-particle slide. The difference between the NS and TPS paths is subtler and has to do with the efficiency by which these methods sample path space. TPS uses shooting moves that run both forward and backward. When the shooting point is chosen near the transition state and runs (backward) toward the initial state, there is a good chance of finding an alternative initial state. The backward trajectories allow TPS to efficiently decorrelate the initial state. NS is based entirely upon forward trajectories. The initial point of the trajectory samples a Boltzmann distribution around the initial state, and without backward shooting moves, it is not able to jump between initial states separated by high barriers. It is this inefficient sampling of the initial state which keeps our NS simulation in the correct compact minimum and yields a rate which is closer to the TST rate for the process of interest (the three-particle slide).

To verify that our TPS rate calculations were inconsis-

TABLE III. LJ rate constants at 95% confidence for each method at equal computational cost but this time with a second OP that correctly isolates the initial state. The headings are the same as in Table II.

| OP | Method | $\dot{p}(t\vert\tau)$ | $P(\tau)/10^{-13}$ | $k_{AB}/10^{-13}$ |
|---|---|---|---|---|
| $\lambda_p,\ \lambda_r$ | TPS | 0.39 | 8.2 | $3.19 \pm 0.29$ |
| | NS | 0.39 | 7.9 | $3.08 \pm 0.26$ |

tent due to an OP which did not uniquely define the desired compact initial state, we repeated our calculations using the new definition $\lambda_r < 0.05$. As before, this value was chosen to be outside of fluctuations from a long thermal trajectory. Since this definition explicitly selects configurations which are close to the compact configuration, any path that does not begin inside this true initial state is rejected from the sampling. When the initial and final states were defined by $\lambda_p < 0.1$ and $\lambda_r < 0.05$, respectively, the rates found from NS and TPS (see Table III) are in statistical agreement with each other and much closer to the hTST rate.

## IV. DISCUSSION AND CONCLUSIONS

Most calculations of rare event rates rely on some assumed low-dimensional collection of coordinates that partition phase space into reactants and products to capture the underlying mechanism of reaction. Once such a set of coordinates is assumed, the free energy surface can be constructed and the reaction pathways uncovered by examination of the surface. One of the key problems with this approach is its sensitivity to the choice of coordinates.[7,21,22] The full configuration (or phase) space contains many dimensions so that one typically resorts to intuition for selecting OPs. TPS has afforded one means of testing the choice of low dimensional coordinates on which the free energy is projected.[23,24] Reactive trajectories can be used to explore the real multidimensional landscape so that a comparison with the low dimensional projection can be made. We have demonstrated here that even when it is possible to calculate the rate constant, the evidence of a failing OP can be subtle. For the simple seven-particle system that we considered here, it was possible to inspect individual reactive paths visually to discern whether or not they reacted as expected. In large systems where a simple description in terms of an OP is even more important, such inspection will be more difficult.

[1] C. Dellago, P. G. Bolhuis, and D. Chandler, J. Chem. Phys. **108**, 9236 (1998).
[2] L. Y. Chen and S. C. Ying, Phys. Rev. B **60**, 16965 (1999).
[3] R. Elber and D. Shalloway, J. Chem. Phys. **112**, 5539 (2000).
[4] T. S. van Erp, D. Moroni, and P. G. Bolhuis, J. Chem. Phys. **118**, 7762 (2003).
[5] R. J. Allen, D. Frenkel, and P. R. ten Wolde, J. Chem. Phys. **124**, 024192 (2006).
[6] K. N. Kudin and R. Car, J. Chem. Phys. **122**, 114108 (2005).
[7] A. Berezhkoviskii and A. Szabo, J. Chem. Phys. **122**, 014503 (2005).
[8] B. Ensing, A. Laio, M. Parrinello, and M. L. Klein, J. Phys. Chem. B **109**, 6676 (2005).
[9] D. J. Wales, Mol. Phys. **100**, 3285 (2002).
[10] G. E. Crooks and D. Chandler, Phys. Rev. E **64**, 0261091 (2001).
[11] B. M. Dickson, J. Chem. Phys. **127**, 064106 (2007).
[12] H. Eyring, J. Chem. Phys. **3**, 107 (1935).
[13] E. Wigner, Trans. Faraday Soc. **34**, 29 (1938).
[14] E. Vanden-Eijnden and F. A. Tal, J. Chem. Phys. **123**, 184103 (2005).
[15] G. Henkelman and H. Jónsson, J. Chem. Phys. **111**, 7010 (1999).
[16] G. Henkelman, B. P. Uberuaga, and H. Jónsson, J. Chem. Phys. **113**, 9978 (2000).
[17] D. Chandler, J. Chem. Phys. **68**, 2959 (1978).
[18] M. P. Allen and D. J. Tildesley, *Computer Simulation of Liquids* (Oxford University Press, New York, 1987).
[19] C. Dellago, P. G. Bolhuis, F. S. Csajka, and D. Chandler, J. Chem. Phys. **108**, 1964 (1997).
[20] L. Y. Chen and N. J. M. Horing, J. Chem. Phys. **124**, 164102 (2006).
[21] S. Yang, J. N. Onuchic, and H. Levine, J. Chem. Phys. **125**, 054910 (2006).
[22] L. Huang and D. Makarov, J. Chem. Phys. **128**, 114903 (2008).
[23] J. E. Basner and S. D. Schwartz, J. Am. Chem. Soc. **127**, 13822 (2005).
[24] R. J. Dimelow, R. A. Bryce, A. J. Masters, I. H. Hillier, and N. A. Burton, J. Chem. Phys. **124**, 114113 (2006).